García-Junceda, A.; Sáez, I.; Deng, X.X.; Torralba, J.M. (2018). Development of a novel Cr-based hard composite processed by spark plasma sintering. *Metallurgical and Materials Transactions A*, 49(4), pp.: 1363-1371.

DOI: https://doi.org/10.1007/s11661-018-4477-7

Development of a Cr-based hard composite processed by spark plasma sintering

A. García-Junceda[a,*], I. Sáez[b], J.M. Torralba[b]

[a] IMDEA Materials Institute, Calle Eric Kandel 2, 28906 Getafe, Madrid, Spain.

[b] Universidad Carlos III Madrid, Av. Universidad 30, 28911 Leganés, Madrid, Spain.

*Corresponding author at: IMDEA Materials Institute, Calle Eric Kandel 2, 28906 Getafe, Madrid, Spain. Tel: +34 91 549 34 22. Fax number: +34 91 550 30 47.

E-mail addresses: andrea.garcia.junceda@imdea.org (A. García-Junceda), 100018812@uc3m.es (I. Sáez), torralba@ing.uc3m.es (J.M. Torralba).

Abstract

This investigation analyzes the feasibility of processing a composite material comprising WC particles randomly dispersed in a matrix in which Cr is the main metallic binder. Thus, a new composite material is processed using a commercial, economic and easily available Cr-based alloy, assuming that there is a certain Cr solubility in the WC particles acting as reinforcement. The processing route followed includes mechanical milling of the powders and consolidation by spark plasma sintering.

Keywords: composite; Cr-based; powder metallurgy; mechanical milling; spark plasma sintering; microstructure.

1. Introduction

Hard composites exhibit a microstructure comprising a metallic matrix (usually Fe, Co, or Ni alloys) and an adequate proportion of hard compounds including carbides, borides or silicides [1]. These materials are especially suitable for wear resistance applications, in which corrosion resistance is also needed, such as grinding balls and tools, spikes, plungers, seal rings, etc. [1] In the last decades, there has been a continuous improvement of compositions and manufacturing techniques leading to a better performance of hard composite materials in order to use them in new applications [2]. Apart from these technological improvements, there is a recent health demand in the field of hard composite materials concerning the partial or total replacement of the frequently used Co binder by other metallic alloy less toxic, more economic and with lower cost fluctuation [3]. This new trend is due to the fact that the inhalation of Co particles can produce an interstitial lung disease [4] and both Co powder and Co hardmetal have been included as "reasonably anticipated to be human carcinogens" in the 14th report on carcinogens on November 2016 [5]. Other transition metals, such as Fe and Ni, have been employed in a limited extent as alternative alloys to Co. Ni-based hard materials have been extensively studied considering their good corrosion resistance [6]. However, the formation of undesirable graphite during cooling is one of the main drawbacks in Ni-based systems [2]. In addition, Ni compounds and metallic Ni have also been listed by the National Toxicology Program (NTP) as “known to be human carcinogens” and “reasonably anticipated to be human carcinogens", respectively [5]. On the other hand, Fe-based systems (FeNi, Fe/Ni/Co, FeMn, FeCr) have been used in hard materials since the early 1920´s due to their reduced price, good availability and low toxicity [7-10]. However, some of these studies have mentioned the inconvenience

of simultaneously obtain good hardness and toughness values in Fe-based hard composites compared to those obtained in WC-Co systems [7,8,10]. The first Fe-W-C ternary phase diagram was obtained in 1936, and it demonstrated the difficulty of avoiding the high thermodynamically stable brittle M_6C eta-phase during sintering, reducing the mechanical properties of these hard materials [11-13]. Another disadvantage of this system is the fact that Fe dissolves a much lower quantity of WC than Co, at their respective eutectic temperatures [2]. On the other hand, it is not possible to find studies in the literature (to the knowledge of the present authors) assessing the possibility of using a sintered Cr-based alloy combined with a WC reinforcement for wear resistance applications, as is the case of the current investigation. Nevertheless, it is possible to find some investigations referred to the addition of small quantities of Cr as metallic Cr, Cr_3C_2 or Nichrome (Ni-18Cr), in order to increase the corrosion resistance of Ni- or Fe- or Co-based hardmetals or to avoid the growth of the WC grains in the case of WC-Co hardmetals [14-16]. There is a work particularly remarkable, in which Rezai-Sameti *et al.* studied the effect of the current density, used during electrodeposition, on the final nanostructure of a Cr-WC composite coating introduced for increasing the microhardness and wear resistance of a steel [17]. Although detailed studies concerning the chromium solubility in WC lattice do not exist, the C-Cr-W phase diagram suggests that a certain solubility should exist [18] and some authors have reported the existence of a small incorporation of Cr in the WC lattice [19-21].

In this investigation, the aim is to analyze the viability of processing a new Cr-based hard composite, using a commercial, economic and easily available Cr-Fe metallic matrix and WC acting as reinforcement. Attending to the above mentioned published studies, analyzing the beneficial effects of adding small quantities of metallic Cr in

composite materials formed by a Fe or Ni or Co matrix on the wear and corrosion properties [14-17], it might be also expected good resistance properties for this new Cr-based hard composite. In addition, the tungsten carbide phase will be responsible for properties such as hardness and it will also have a strong influence on the wear resistance of the Cr-based composite material [22]. On the other hand, the small fraction of iron within the raw powders will contribute to reduce the temperature needed during the sintering and to increase slightly the ductility of the hard composite. Thus, in this paper a new WC-CrFe composite is processed by a powder metallurgy route including mechanical milling (MM) of two commercial powders and consolidation by spark plasma sintering (SPS), which is a powerful technique to process hard composite materials in a short period of time, contributing to the limitation of the grain size of the different microconstituents. Since these authors did not find previous studies showing the microstructure achieved during the milling of high fractions of Cr-based powders with WC powders, a deep microstructural and crystallographic study during the mechanical milling is performed in this investigation. Moreover, after SPS new phases are formed and their characterization is carried out in order to analyze and explain the transformations taking place during the SPS process.

2. Materials and Methods

2.1. MM and characterization of the powders

The raw powders used in this investigation comprise Cr-Fe alloy (71.4Cr-28.1Fe-0.4Si-0.04C-0.03N-0.02P-0.004S in wt.%) provided by Höganas (Sweden), WC (purity 99,7 wt.%) manufactured by Alfa Aesar (USA) and stearic acid acting as process control

agent (PCA) and supplied by Sigma Aldrich (USA). The volume fraction of WC is fixed at 30%, so a mixture with 50 wt.% of pure WC and 50 wt.% of CrFe alloy is introduced in a Fritsch Pulverissette 6 planetary ball mill. The mixture is milled for 10 h under protective argon atmosphere and 0.5 wt.% of PCA is added to the mixture. The rotation speed is 350 rpm with a ball-to-powder weight ratio of 10:1 and 10 mm ball diameter. The vessel and balls were supplied by Fritsch and their nominal composition is 93.8CW-6.0Co-0.2 others (in wt.%). In order to follow the evolution of the milled powders, samples are taken each two hours of milling time. The microstructural evolution of the particles is analyzed in the cross-section of the specimens by Scanning Electron Microscopy coupled to Energy Dispersive X-ray spectroscopy (spot analyses with a stationary beam) at an accelerating voltage of 20 kV (SEM-EDX, EVO MA15-Oxford INCA 330). The particle size distribution is determined by a laser diffraction analyzer (Mastersizer 2000). Finally, the structural characterization of the powders is performed using the Cu kα radiation of a Phillips X´pert diffractometer and applying the Scherrer method to obtain the values of crystallite size and lattice strain [23].

2.2. SPS and characterization of the consolidated Cr-based hard composite

The 10 h milled WC-CrFe powders are consolidated by SPS using a HPD-25 equipment (FCT System GmbH, Germany). The particles are poured into a cylindrical graphite die (20 mm in diameter) and heated in a vacuum chamber (10^{-3} Pa). A pure tungsten foil (>99.97%), with a thickness of 25 μm, is employed to suppress carbon contamination and to avoid the attachment of the consolidated composite to the die/punches [24]. The sintering temperature selected is 1523 K (1250 ºC), with a heating rate of 100 K/min (ºC/min) and a dwell time of 10 min, followed by furnace cooling. The temperature is

measured with a Pyro-Top pyrometer. The applied pressure during the consolidation is 80 MPa. The simultaneous application of electrical current and mechanical pressure promotes the atoms mobility, leading to a solid-state sintering fully activated [25]. In order to analyze the microstructure and the composition of the sintered SPS sample, SEM studies are accomplished by means of Field Emission Gun Microscopy (FIB-FEGSEM dual-beam microscope, Helios Nanolab 600i FEI). In addition, FIB samples are obtained to characterize in more detail the consolidated WC-CrFe composite material using a FEG S/TEM microscope (Talos F200X, FEI) working at 200 kV and equipped with a chemical analysis system via EDX for elemental mapping analysis. On the other hand, the analysis of the phases is performed by X-ray diffraction (XRD), using the Cu kα radiation of an Empyrean PANalytical diffractometer. Moreover, to complete the study of the microstructure and the distribution of the tungsten carbide phases, EBSD patterns are obtained in the FEG microscope equipped with the HKL Channel 5.0 acquisition and analysis software package, provided by Oxford Instruments. The acquisitions are conducted at an accelerating voltage of 15 kV and a beam current of 5.5 nA. The selected step size is 0.04 μm and the grain boundary misorientation angles above 5º. On the other hand, the density of the sample is measured by the Archimedes method [26]. Hardness measurements are performed in the consolidated sample, applying a load of 30 kg during 10 s in a NEXUS 4000 tester equipped with a Vickers diamond indenter. The study of the fracture toughness, based on the Palmqvist indentation toughness test, is carried out on the SPS Cr-based composite as indicated by the international standard ISO 28079 [27]. Following this standard, the polished hard material is indented at 30 kgf, with the Vickers hardness testing machine, and the measurement of the individual cracks length from the

indentation corner to the crack tip for each of the four cracks is performed to calculate the Palmqvist fracture toughness, W_K [27].

3. Results and Discussion

3.1. Characterization of the raw powders

The Cr-Fe powder shown in the images of Fig. 1(a) exhibits an irregular morphology, whereas WC powders present polygonal shape (Fig. 1(b)). The particle size of WC powder is slightly bigger and with a narrower distribution than Cr-Fe powder (Fig. 2).

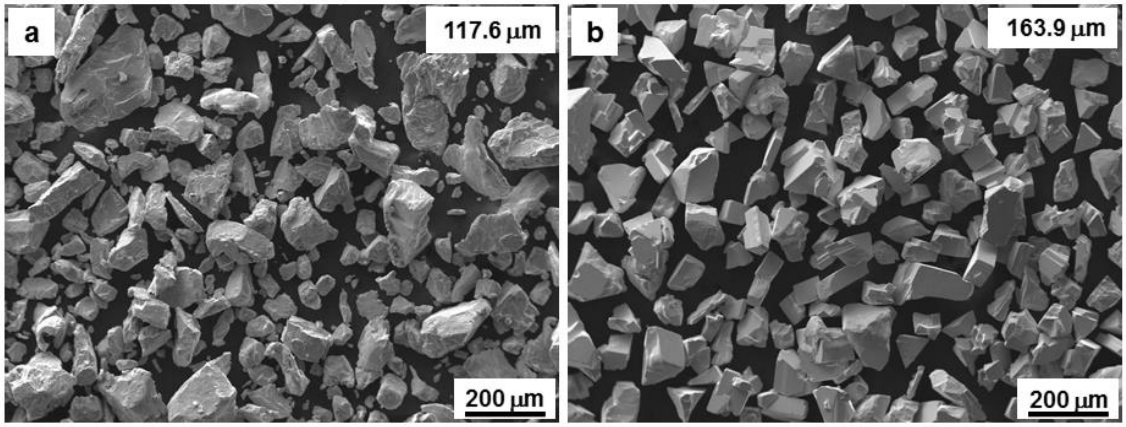

Fig. 1. SE-SEM (Secondary Electron -SE-) micrographs of the raw powders including D_{50} values: (a) Cr-Fe, (b) WC.

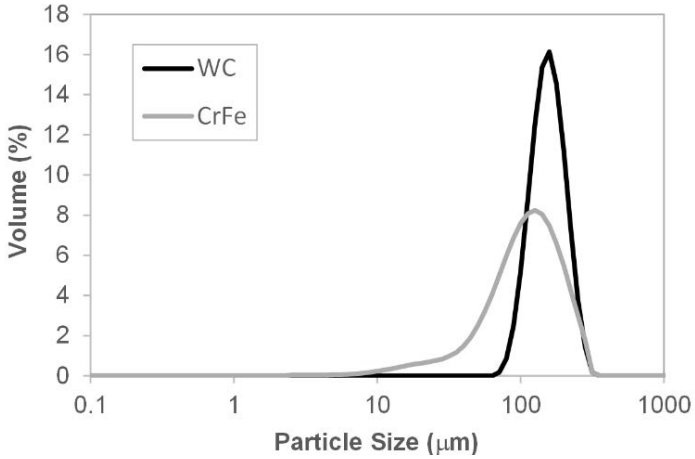

Fig. 2. Particle size distribution of the raw powders.

3.2. Characterization of the MM Cr-based hard composite powders

In order to analyze the evolution of the morphology, microstructure and composition of the MM powders, samples are taken each two hours of milling time. The micrographs of Fig. 3 show this evolution, where the grey regions correspond to the metallic matrix and the white regions are formed by the WC reinforcement. After 2 hours of MM, two phases are still clearly distinguishable: big grey areas of deformed Cr-Fe phase and brittle fragmented WC particles (Fig. 3(a)). At this stage, only some carbides have been incorporated into the matrix. However, after 4 h of milling time, it is possible to detect some laminar zones formed by the ductile metallic alloy and the WC fragments (Fig. 3(b)), as a result of two phenomena occurring at the same time: the welding of the deformed particles of Cr-Fe and the insertion of the reinforcement in the middle of two or more ductile particles during the ball collision. The processing involves repeated cold welding, fragmentation and dynamic recrystallization. Finally, the MM leads to a fine WC reinforcement randomly dispersed within the matrix. Moreover, the particles tend to be rounder and finer with the increase of the milling time, as shown in Fig. 3(c), 3(d) and 3(e). The evolution of the powder morphology as a function of the time follows the expected progression of a brittle-ductile system reported by Fogagnolo *et al.* [28]

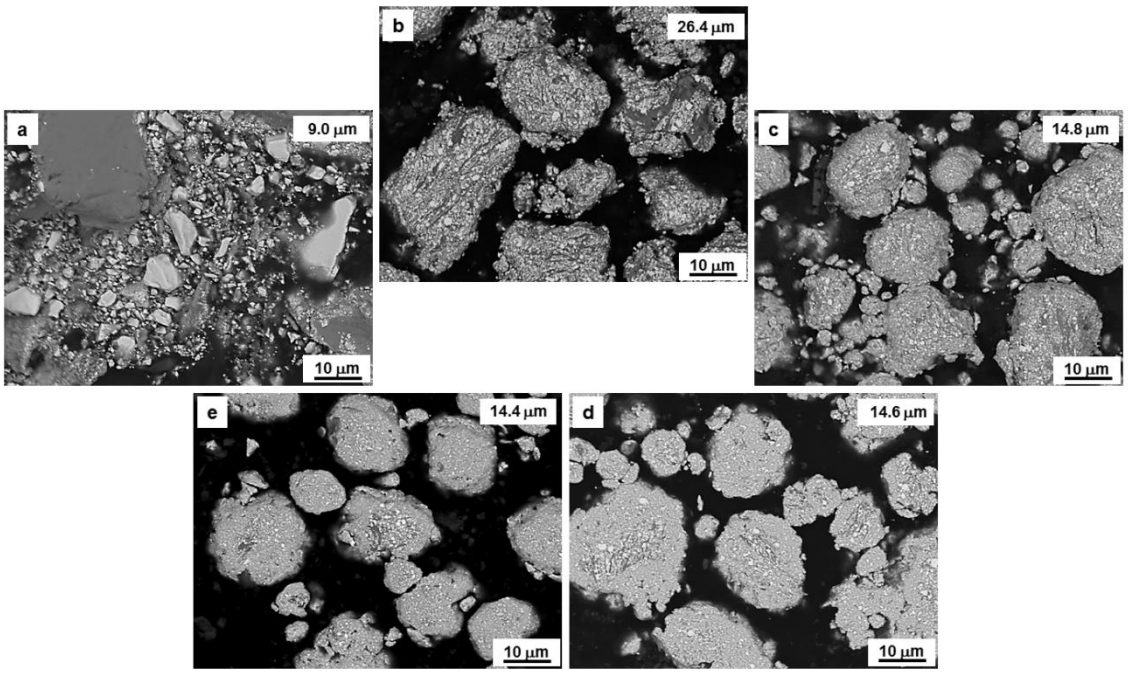

Fig. 3. BSE-SEM (Backscatter Electron -BSE-) images showing the morphological and microstructural evolution of the WC-CrFe particles after: (a) 2 h, (b) 4 h, (c) 6 h, (d) 8 h, (e) 10 h of milling time. Evolution of the D_{50} values.

In addition, a XRD study is performed in order to help in the selection of the most optimum milling time. The XRD patterns showed in Fig. 4 do not reveal any phase transformation taking place during mechanical milling. Consequently, only WC, Cr and Fe phases are detected and all patterns exhibit the same peaks corresponding to these three phases. The crystallite size and the lattice strain are determined from these patterns, considering that the milling induces structural changes in the hexagonal WC lattice. The results presented in the graphics of Fig. 5 point out the decrease of the crystalline coherence zone with the milling time and, consequently, the decrease of the crystallite size from 12 to 7 nm, as a result of the generation of a high density of dislocations. The refinement of the crystallite size reaches a saturation level after 8 hours of milling, indicating that a further refinement becomes quite difficult for this system. This limit in the grain size is dependent on the melting temperature and the

activation energy for self-diffusion of the material [29]. Thus, the higher the melting temperature and/or the activation energy for self-diffusion of the composite, the lower normalized minimum grain size achieved [29]. On the other hand, the MM process increases the lattice distortions because of the incorporation of Cr and Fe to the hexagonal WC lattice, generating an increase of the lattice microstrain from 0.520 to 0.975%. The steady-state, attained in the lattice strain after 8 hours of milling, is due to the balance achieved between the rate of cold welding and the rate of fracturing of the particles being milled, whereas the plastic deformation plays a negligible role at this stage [30]. Both parameters, small crystallite size and high lattice strain, are of importance to obtain a nanostructured system since the sintering is a process thermally activated, in which the crystal growth begins when the internal strain decreases under a certain value that will depend on the material [31]. In the case of the present study, the values obtained for the crystallite size and the strain are in fully accordance with the values reported by Molinari *et al.* [32] for different equivalent metallic systems. The subsequent use of SPS as a forming process will allow the nanostructured system to be retained to some extent after the consolidation.

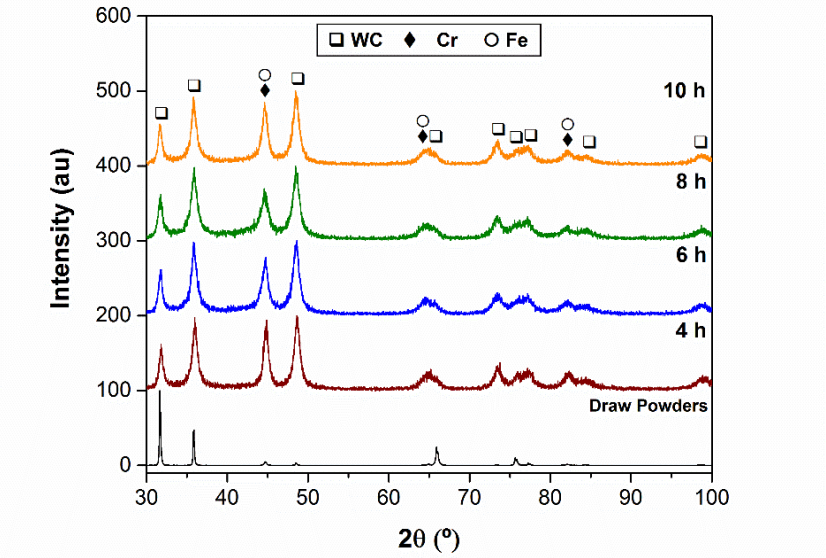

Fig. 4. XRD patterns showing the crystallographic evolution of the WC-CrFe powder with the milling time.

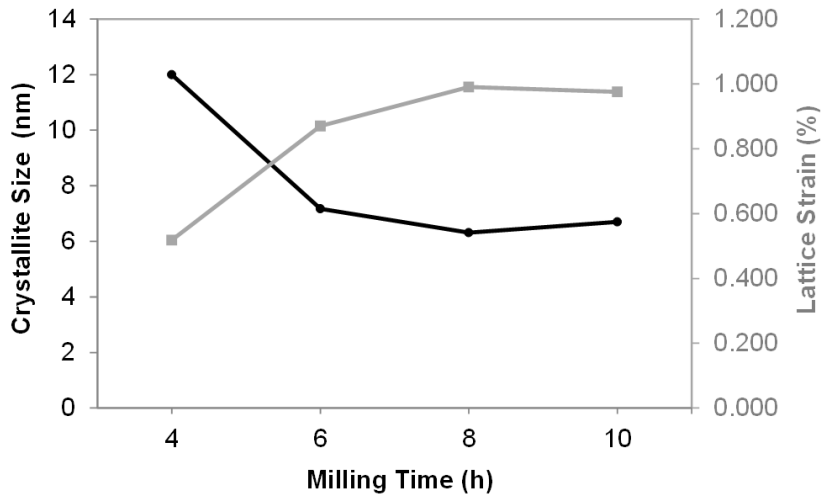

Fig. 5. Crystallite size and lattice strain evolution during MM of the WC-CrFe powder.

After all these analyses, the 10 h MM WC-CrFe powder is selected as the most suitable for the subsequent consolidation by SPS since it is fine, round, homogeneous without chromium carbides in their microstructure and with adequate crystallographic parameters for the subsequent consolidation.

3.3. Consolidated SPS Cr-based hard composite

A SEM micrograph showing the microstructure of the WC-CrFe composite obtained after the consolidation by SPS at 1523 K (1250 ºC) is shown in Fig. 6(a). The microstructure exhibits white islands, corresponding to tungsten carbide phases, which have different sizes and shapes along the matrix. The sintering has led to a tungsten carbide grain coarsening from the MM powder to the SPS sample. The length of the tungsten carbide islands in the SPS sample is between 0.1-2.0 μm. On the other hand, the grey areas, which are free of reinforcement, correspond to the Cr-based alloy. The results of the EDX mapping analysis indicate that the target composition (calculated considering the elemental wt.% introduced during the milling of the powders) has been

reached (Fig. 6(b)). However, the carbon content is higher than expected, probably due to a contamination coming from the WC-Co vessel used for milling. In addition, some small and equiaxed pores are present in the microstructure, leading to a relative density value of 95%. The microstructure is heterogeneous since the size of the WC varies along the Cr-based matrix and it is possible to find relatively big regions without any reinforcement. In order to study in more detail the microstructure and the composition of this hard composite, TEM coupled to EDX elemental mapping analysis, XRD diffraction studies and EBSD acquisitions are performed. The grain morphology and grain size of the different phases involved in the SPS WC-CrFe composite are shown in Fig. 7. The high-angle annular dark-field (HAADF) image shows the tungsten carbide islands in white and the Cr-based matrix in grey (Fig. 7(a)). In addition, a bright-field (BF) micrograph taken in the same area exhibits the grain shape and the size of both the reinforcement and metallic alloy (Fig. 7(b)). The grain size of the Cr-based constituent, determined from Fig. 7(b), ranges from 0.2 to 0.9 μm and is slightly smaller than the grain size of the tungsten carbide islands, which varies between 0.1-2.0 μm. Thus, this investigation highlights the possibility of obtaining fine grain sizes within a Cr-based hard composite processed by SPS. From Fig. 7, it is clear that the porosity is mainly located at the grain boundaries, where a higher level of surface energy being the main driving force in the sintering process can be found, indicating that the boundary diffusion was not enough enhanced by the current and pressure applied during the SPS process. The EDX elemental mapping images of Fig. 8 illustrate the existence of a Cr-Fe (purple/blue) matrix and some areas enriched in W (yellow) which can be divided into regions with two different composition: a) regions comprising Cr and W, with lower Cr content than the matrix, b) regions enriched in Fe and W, with higher Fe

contents than the matrix. The regions containing Cr-tungsten compounds are in minority compared with the Fe-tungsten areas.

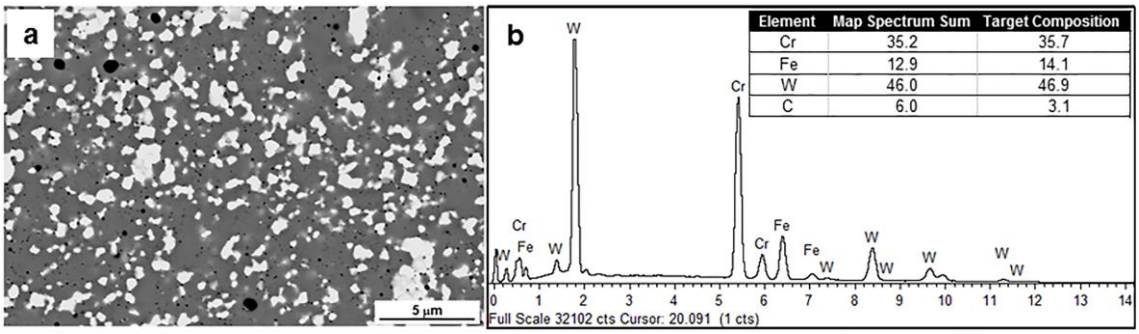

Fig. 6. (a) BSE-SEM image and (b) EDX analysis of SPS WC-CrFe composite (in wt.%).

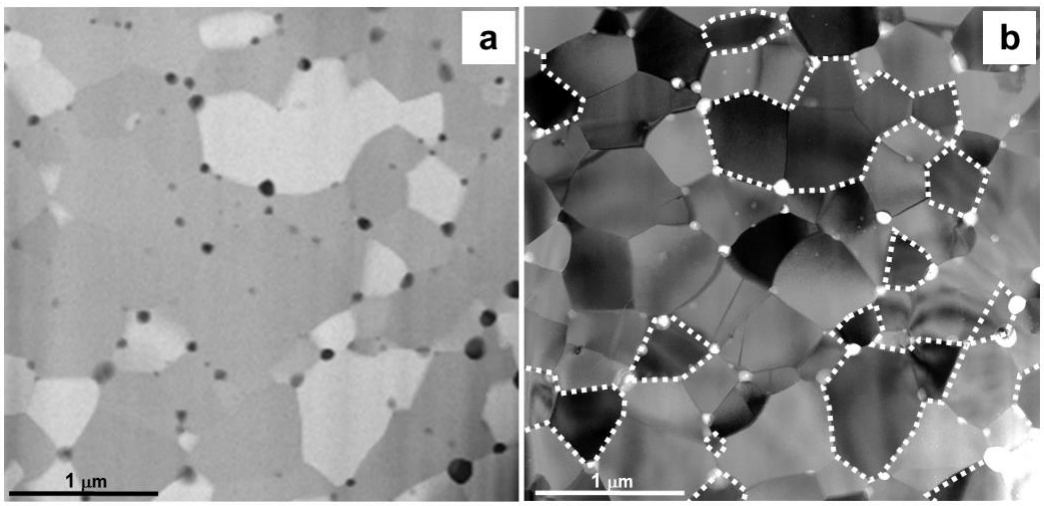

Fig. 7. Microstructure of the SPS WC-CrFe composite: (a) HAADF-STEM image, (b) BF-TEM image (the dotted lines indicate the tungsten carbide islands).

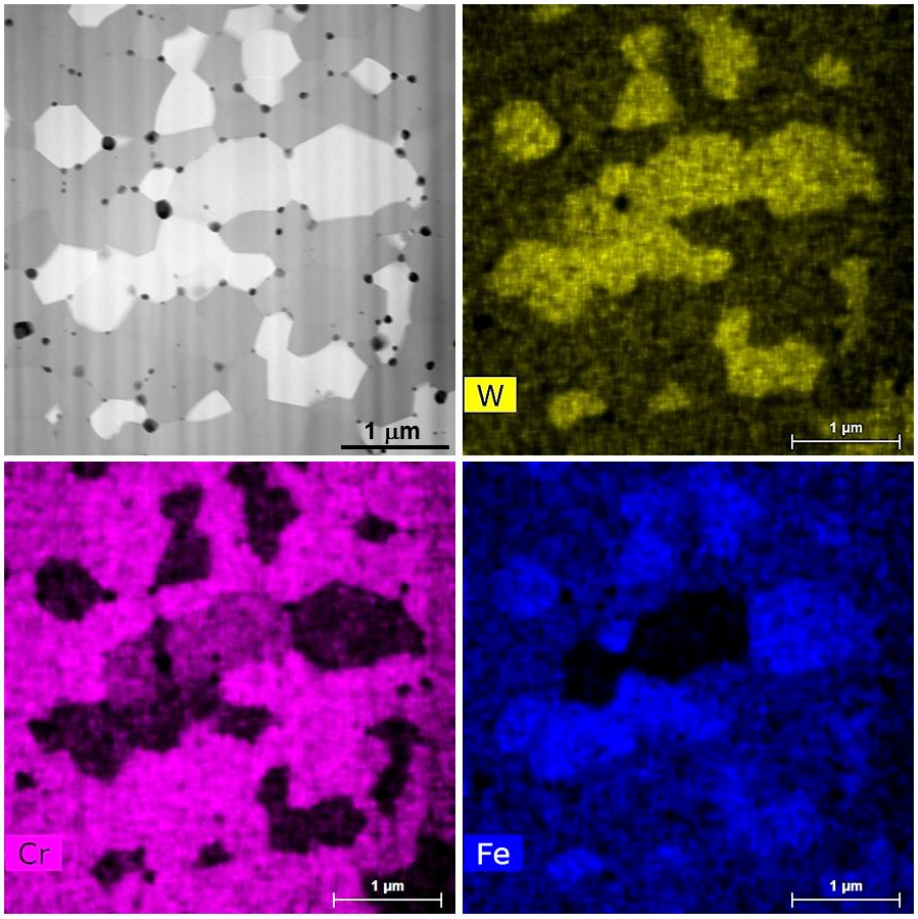

Fig. 8. EDX elemental mapping images of SPS WC-CrFe composite, showing W (yellow), Cr (purple), Fe (blue) and the corresponding HAADF-STEM image. Color figures are retained in online version.

Within the aim of determining the composition and stoichiometry of these phases existing in the consolidated Cr-based hard composite, an X-ray diffraction pattern is obtained (Fig. 9). The identification of the different peaks of this pattern confirms the existence of a Cr-Fe matrix and four different ternary carbides acting as reinforcement, identified as $Fe_{21}W_2C_6$, Fe_3W_3C, Fe_2W_2C and $(W,Cr)_2C$. Some previous research works of other authors on Fe-W-C-Cr systems suggested the formation of undesirable brittle eta-carbides, mainly M_6C and $M_{12}C$, as a result of a chemical reaction, and other brittle carbides comprising $M_{23}C_6$, M_7C_3, M_3C_2 and M_3C since both Fe and Cr exhibit a strong affinity to carbon (M= Cr, Fe and W) [2,12,33,34]. Goldschmidt showed the first

schematic quaternary C-Cr-Fe-W system in 1952 [35], in which the replacement of all the Cr in the $Cr_{23}C_6$ led to the carbide with stoichiometry $Fe_{21}W_2C_6$ detected in the present study. The Fe_3W_3C is a typical brittle eta-phase (M_6C) found in the ternary system Fe-W-C [36] and difficult to avoid during sintering due to its high thermodynamic stability [11]. The Fe_2W_2C phase has been reported by Luo *et al.* as a brittle carbide phase found after microwave sintering of a steel bonded tungsten carbide due to the phase transition between WC and Fe [37]. Finally, the presence of $(W,Cr)_2C$ phases in the sintered Cr-based hard composite, previously found by other authors as an intermediate product in the carburization of a W + Cr_3C_2 + C mixture [20], experimentally confirms the solubility of the Cr in the hexagonal WC lattice. The ternary phase diagram comprising C-Cr-W suggests a small solubility at 1623 K (1350 ºC) [38] and other authors have reported a certain solubility of Cr in WC for sintering studies at higher temperatures, ranging from 1673 K to 2023 K (1400 to 1750 ºC) [18,19]. Thus, this investigation points out the existence of certain solubility of Cr in WC at the sintering temperature of 1523 K (1250 ºC). It is worth mentioning that all the initial WC has transformed to Fe or Cr tungsten carbides with different stoichiometries and sizes. The space group and the formula unit per cell adopted by the thermodynamically stable carbides are different (Fm-3m and Z=4 for $Fe_{21}W_2C_6$, Fd-3m and Z=16 for Fe_3W_3C, Fd-3s and Z=24 for Fe_2W_2C and $P6_3/mmc$ and Z=2 for $(W,Cr)_2C$) [39,40], so the analysis of the different phases by EBSD allows to determine their location within the microstructure (Fig. 10). The phases identified in the EBSD map of Fig. 10(b) are in good agreement with the EDX elemental mapping results schematized above, establishing a Cr-Fe matrix (red and orange, respectively) and endorsing the existence of tungsten carbide islands (white color in Fig. 10(a)), randomly distributed along the matrix, identified as mixtures of $Fe_{21}W_2C_6$ (blue), Fe_3W_3C (green),

Fe_2W_2C (yellow) and well defined areas formed by $(W,Cr)_2C$ (purple). With respect to the iron carbides, the $Fe_{21}W_2C_6$ is the majority phase (18 vol.%), followed by Fe_3W_3C (3.6 vol.%) and Fe_2W_2C (2.5 vol.%). These results are consistent with the stability sequence of Fe-W-C ternary compounds suggested by Liu *et al.* [39] The $(W,Cr)_2C$ compound, with a hexagonal crystal structure in which the Cr and the W atoms occupy interstitial positions [40], is the second majority carbide (5.9 vol.%), consequently its thermodynamic stability may be higher than those exhibited by Fe_3W_3C and Fe_2W_2C. It is clear that in this system involving W, C, Cr and Fe, different compounds can be developed during the sintering process, and the consequence is a promising sintering behavior through a good selection of the sintering parameters.

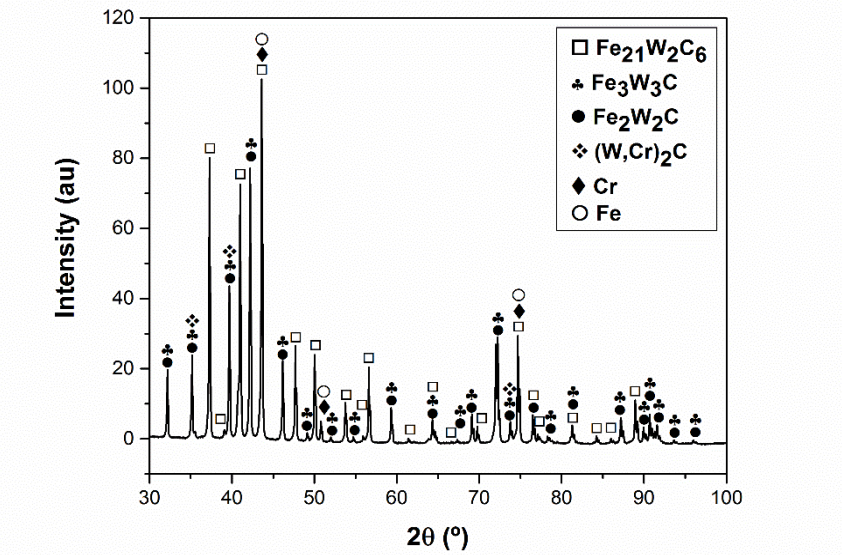

Fig. 9. XRD pattern of the SPS WC-CrFe composite.

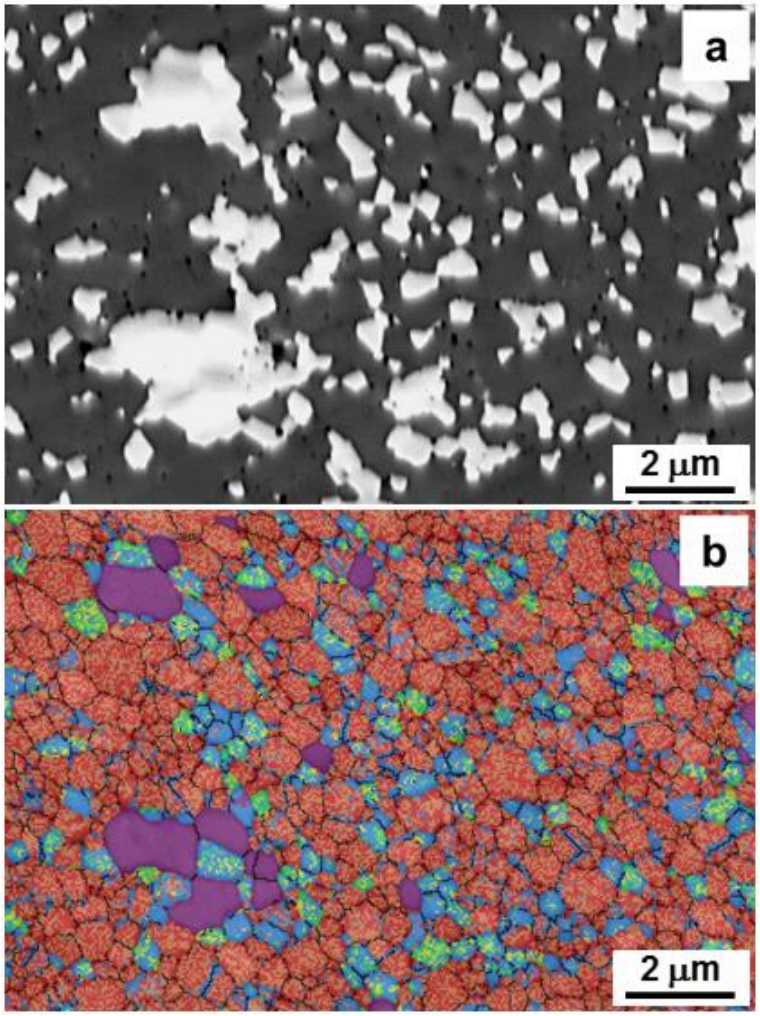

Fig. 10. SPS WC-CrFe composite: (a) BSE-SEM image, (b) Multiphase EBSD mapping showing Cr-red, Fe-orange, $Fe_{21}W_2C_6$-blue, Fe_3W_3C-green, Fe_2W_2C-yellow, $(W,Cr)_2C$ - purple. For interpretation of the phases to color, the reader is referred to the web version of this article.

As a first approach to assess the mechanical properties of the SPS WC-CrFe composite, Vickers hardness is measured, given as a result (1479 ± 47) HV30, which represents a promising value located in the upper range of other hard composites in which the hardness values range from 700 to 1800 HV30 [41, 42]. The Palmqvist fracture toughness achieved has a low value, $W_K = (3.4 \pm 0.1)$ $MNm^{-3/2}$. This fracture toughness value is within the range of those obtained by other semi-brittle materials with data

ranging from 0.3 to 8 $MNm^{-3/2}$ [43]. The low fracture toughness can be attributed to two factors acting together and conferring brittleness to this Cr-based composite: a) the porosity found in the specimen (relative density of 95%) and b) the presence of the brittle ternary carbides previously described. Through thermo-dynamical studies of the WC-Cr-Fe system it will be possible to obtain suitable information to optimize the development of these new hard composites. Phase equilibria diagram studies are currently ongoing in order to sinter WC-CrFe composite materials with an optimized composition by adding extra carbonyl iron and graphite powders. Although this compositional optimization will increase the price of the final composite, it is worth to achieve a new material with a higher density and limited formation of undesirable phases. The phase equilibrium is characterized by the existence of two phase region: a face-centered cubic crystal system and WC (FCC+WC) [2], limiting the presence of brittle carbide phases and, therefore, leading to the improvement of the mechanical properties. Furthermore, the experimental processing conditions programmed during SPS (heating rate, temperature and pressure) will be improved in order to achieve near full-density samples. The presence of porosity in the material may be detrimental for the future wear resistance of Cr-based composite materials since these pores act as stress raisers and facilitate the crack initiation when an external force is applied [44,45]. Despite these drawbacks, this investigation confirms the feasibility of consolidating a new hard composite, formed by a Cr-based metallic matrix and WC, using a field-assisted sintering technique (FAST) that limits the grain growth, as is the particular case of SPS.

4. Conclusions

- The mechanical milling of Cr-Fe and WC powders during 10 h leads to a fine and round WC-CrFe powder, with homogeneous distribution of WC throughout the metallic matrix and favorable crystallographic parameters for the subsequent consolidation step. Cr and/or Fe carbide phases are not detected in these powders.
- $M_{23}C_6$, M_6C and M_4C carbides (being M=Fe and W) are found after sintering at 1523 K (1250 ºC) by SPS.
- M_2C carbides (being M=Cr and W) are identified within the hard composite. In particular, hexagonal $(Cr,W)_2C$ is found in well-defined areas, which suggests certain solubility of Cr in WC.
- Hexagonal mono WC is not detected after sintering, due to its complete transformation into the previously mentioned ternary Fe and Cr tungsten carbides.
- The grains are fine and smaller than 2 μm for all the constituents forming the WC-CrFe composite, due to the relative low temperature and short processing time needed for the consolidation by SPS.
- The viability of using the SPS technique for sintering a Cr-based hard composite with high hardness, starting from commercial feedstock powders and avoiding the use of carcinogenic elements, is assessed. Further thermo-dynamical studies and sintering treatments are being performed in order to optimize the composition, avoiding the formation of brittle carbide phases, and to obtain full-density SPS samples.

Acknowledgements

This research did not receive any specific grant from funding agencies in the public, commercial, or not-for-profit sectors. The authors wish to express their gratitude to the Nanomaterials and Nanotechnology Research Center (CINN), for providing the

facilities to carry out the Spark Plasma Sintering experiments, and to Dr. Miguel Castillo-Rodríguez and Marta Cartón-Cordero for their unconditional experimental and technical support.

References

[1] A. Zerr, H. Eschnauer and E. Kny, Hard Materials: *Ullmann's Encyclopedia of Industrial Chemistry*, Ed. Wiley, 2012, pp. 1-21.

[2] C.M. Fernandes and A.M.R. Senos: *Int. J. Refract. Metals Hard Mater*., 2011, vol. 29, pp. 405-418.

[3] C. Liu , Alternative Binder Phases for WC Cemented Carbides, *M.Sc. thesis*, Royal Institute of Technology, Sweden, 2015.

[4] D. Lison and R. Lauwerys: *Toxicol. In Vitro*, 1995, vol. 9, pp. 341-347.

[5] NTP (National Toxicology Program), 2016 Report on Carcinogens, Fourteenth Edition, Research Triangle Park, NC: U.S. Department of Health and Human Services, Public Health Service. https://ntp.niehs.nih.gov/pubhealth/roc/index-1.html. Accessed 27 March 2017.

[6] S. Raghunahan, R. Caron and P. Sandell: *Adv. Mater. Process.*, 1996, vol. 4, pp. 21-23.

[7] C.M. Fernandes, V. Popovich, M. Matos, A.M.R. Senos and M.T. Vieira: *Ceram. Int.*, 2009, vol. 35, pp. 369-372.

[8] C. Hanyaloglu, B. Aksakal and J.D. Bolton: *Mater. Charact.*, 2001, vol. 47, pp. 315-322.

[9] T. Farroq and T.J. Davies: *Int. J. Powder Metall.*, 1991, vol. 27, pp. 347–355.

[10] W.D. Schubert, M. Fugger, B. Wittmann and Useldinger: *Int. J. Refract. Metals Hard Mater.*, 2015, vol. 49, pp. 110-123.

[11] S. Takeda: *Sci. Rep. Töhoku Univ. Honda Anniversary Volume*, 1936, pp. 864-881.

[12] T.W. Penrice: *Carbide Tool J*, 1988, vol. 20, pp. 12-15.

[13] P. Gustafson: *Metall. Trans. A*, 1988, vol. 19A, pp. 2547-2554.

[14] K. Shi, K. Zhou, Z. Li, X. Zan and S. Xu, Z. Min: *Int. J. Refract. Metals Hard Mater.*, 2013, vol. 38, pp. 1-6.

[15] V. Bounhoure, S. Lay, S. Coindeau, S. Norgren, E. Pauty and J.M. Missiaen: *Int. J. Refract. Metals Hard Mater.*, 2015, vol. 52, pp. 21-28.

[16] V. Bonache, M.D. Salvador, A. Fernández and A. Borrell: *Int. J. Refract. Metals Hard Mater.*, 2011, vol. 29, pp. 202-208.

[17] M. Rezaei-Sameti, S. Nadali, J. Rajabi and M. Rakhshi: *J. Molec. Struct.*, 2012, vol. 1020, pp. 23-27.

[18] M. Brieseck, M. Bohn and W. Lengauer: *J. Alloys Compd.*, 2010, vol. 489, pp. 408-414.

[19] J. Weidow, S. Johansson, H.-O. Andrén and G. Wahnström: *J. Am. Ceram. Soc.*, 2011, vol. 94, pp. 605–610.

[20] J. Weidow, A. Blomqvist, J. Salomonsson and S. Norgren: *Int. J. Refract. Metals Hard Mater.*, 2015, vol. 49, pp. 36-41.

[21] Z. Tükör, W.-D. Schubert, A. Bicherl, A. Bock and B. Zeiler: *Proceedings 17th International Plansee Seminar 2009*, Plansee Group, Austria, 2009.

[22] Z. Zhao, J. Liu, H. Tang, X. Ma and W. Zhao: *J. Alloys Compd.*, 2015, vol. 632, pp. 729-734.

[23] P. Scherrer, Mathematisch-Physikalische Klasse, 1918, vol. 2, pp. 98-100.

[24] A. García-Junceda, L. Acebo and J.M. Torralba: *Metall. Mater. Trans. A*, 2015, vol. 46A, pp. 3192-3198.

[25] W. Li, E.A. Olevsky, J. McKittrick, A.L. Maximenko and R. M. German: *J. Mater. Sci.*, 2012, vol. 47, pp. 7036–7046.

[26] MPIF Standard 42, Determination of density compacted or sintered metal powder products. Issued 1980, revised 1986.

[27] International standard ISO 28079, Hardmetals-Palmqvist toughness test, 2009.

[28] J.B. Fogagnolo, F. Velasco, M.H. Robert and J.M. Torralba: *Mater. Sci. Eng. A*, 2003, vol. 342A, pp. 131-143.

[29] F.A. Mohamed and Y. Xun: *Mater. Sci. Eng. A*, 2003, vol. 354A, pp. 133-139.

[30] D.R. Amador and J.M. Torralba: *J. Mater. Process. Tech.*, 2003, vol. 143–144, pp. 776–780.

[31] L. Fuentes-Pacheco, M. Campos and J.M. Torralba: *Rev. Metal. Madrid*, 2011, vol. 47, pp. 373-380.

[32] A. Molinari, S. Libardi, M. Leoni and P. Scardi: *Acta Mater.*, 2010, vol. 58, pp. 963-966.

[33] M. Bergström: *Mater. Sci. Eng.*, 1977, vol. 27, pp. 271-286.

[34]. D.V. Suetin and N.I. Medvedeva: *J. Alloys Compd.*, 2016, vol. 681, pp. 508-515.

[35] H.J. Goldschmidt: *J. Iron Steel Inst.*, 1952, vol. 170, pp. 189-204.

[36] M. Bergström: *Mater. Sci. Eng*., 1977, vol. 27, pp. 257-269.

[37] J. M. Luo, Z. Wei, J. L. Xu and L. P. Deng: *Adv. Mater. Res*., 2011, vol. 335-336, pp. 836-840.

[38] P. Villars, A. Prince and H. Okamoto: *Handbook of Ternary Alloy Phase Diagrams*, ASM International, Materials Park, OH, 1995, pp. 9356–9390.

[39] Y. Liu, Y. Jiang, R. Zhou and J. Feng: *Comput. Mater. Sci.*, 2014, vol. 82, pp. 26-32.

[40] E.I. Gladyshevskii, V.S. Telegus, T.F. Fedorov and Y.B. Kuzma: *Russ. Metall.*, 1967, vol. 1, pp. 97-100.

[41] W.D. Schubert, H. Neumeister, G. Kinger and B. Lux: *Int. J. Refract. Metals Hard Mater.*, 1998, vol. 16, pp. 133-142.

[42] A. Akhtar, S. Guo, J.Askari and J. Tian: *J. Univ. Sci. Technol. B*, 2007, vol. 14, pp. 89-93.

[43] W.W. Gerberich, W.M. Mook, C.B. Carter and R. Ballarini: *Int. J. Fract.*, 2007, vol. 148, pp. 109-114.

[44] Y. Mai, B. Cotterell, S.Q. He, Y.B. Ke: *Handbook of Fatigue Crack Propagation in Metallic Structures*, Elsevier, Amsterdam, 1991, pp. 221–246.

[45] D.A. Gerard, D.A. Koss: *Int. J. of Powder Metall.*, 1990, vol. 26, pp. 337-343.

Figure Captions

Fig. 1. SE-SEM (Secondary Electron -SE-) micrographs of the raw powders including D_{50} values: (a) Cr-Fe, (b) WC.

Fig. 2. Particle size distribution of the raw powders.

Fig. 3. BSE-SEM (Backscatter Electron -BSE-) images showing the morphological and microstructural evolution of the WC-CrFe particles after: (a) 2 h, (b) 4 h, (c) 6 h, (d) 8 h, (e) 10 h of milling time. Evolution of the D_{50} values.

Fig. 4. XRD patterns showing the crystallographic evolution of the WC-CrFe powder with the milling time.

Fig. 5. Crystallite size and lattice strain evolution during MM of the WC-CrFe powder.

Fig. 6. (a) BSE-SEM image and (b) EDX analysis of SPS WC-CrFe composite (in wt.%).

Fig. 7. Microstructure of the SPS WC-CrFe composite: (a) HAADF-STEM image, (b) BF-TEM image (the dotted lines indicate the tungsten carbide islands).

Fig. 8. EDX elemental mapping images of SPS WC-CrFe composite, showing W (yellow), Cr (purple), Fe (blue) and the corresponding HAADF-STEM image. Color figures are retained in online version.

Fig. 9. XRD pattern of the SPS WC-CrFe composite.

Fig. 10. SPS WC-CrFe composite: (a) BSE-SEM image, (b) Multiphase EBSD mapping showing Cr-red, Fe-orange, $Fe_{21}W_2C_6$-blue, Fe_3W_3C-green, Fe_2W_2C-yellow, $(W,Cr)_2C$ - purple. For interpretation of the phases to color, the reader is referred to the web version of this article.